The Astrophysical Journal Letters, 821:L26 (5pp), 2016 April 20 doi:10.3847/2041-8205/821/2/L26

SPATIALLY RESOLVED STAR FORMATION MAIN SEQUENCE OF GALAXIES IN THE CALIFA SURVEY

M. Cano-Díaz[1], S. F. Sánchez[1], S. Zibetti[2], Y. Ascasibar[3,4], J. Bland-Hawthorn[5], B. Ziegler[6], R. M. González Delgado[7], C. J. Walcher[8], R. García-Benito[7], D. Mast[9,10], M. A. Mendoza-Pérez[7], J. Falcón-Barroso[11,12], L. Galbany[13,14], B. Husemann[15], C. Kehrig[7], R. A. Marino[16,17], P. Sánchez-Blázquez[3,18], C. López-Cobá[1], Á. R. López-Sánchez[19,20], and J. M. Vilchez[7]

[1] Instituto de Astronomía, Universidad Nacional Autónoma de México, Apartado Postal 70-264, Mexico D.F., 04510, Mexico
[2] INAF-Osservatorio Astrofisico di Arcetri, Largo Enrico Fermi 5, I-50125 Firenze, Italy
[3] Departamento de Física Teórica, Universidad Autónoma de Madrid, E-28049 Madrid, Spain
[4] Astro-UAM, UAM, Unidad Asociada CSIC, Spain
[5] Sydney Institute for Astronomy, School of Physics, University of Sydney, Sydney, NSW 2006, Australia
[6] Universität Wien, Institut für Astrophysik, Türkenschanzstraße 17, A-1180 Wien, Austria
[7] Instituto de Astrofísica de Andalucía (IAA-CSIC), Glorieta de la Astronomía s/n Aptdo. 3004, E-18008 Granada, Spain
[8] Leibniz-Institut für Astrophysik Potsdam (AIP), An der Sternwarte 16, D-14482 Potsdam, Germany
[9] Observatorio Astronómico, Laprida 854, X5000BGR, Córdoba, Argentina
[10] Consejo de Investigaciones Científicas y Técnicas de la República Argentina, Avda. Rivadavia 1917, C1033AAJ, CABA, Argentina
[11] Instituto de Astrofísica de Canarias, Vía Láctea s/n, E-38205 La Laguna, Tenerife, Spain
[12] Departamento de Astrofísica, Universidad de La Laguna, E-38205 La Laguna, Tenerife, Spain
[13] Millennium Institute of Astrophysics MAS, Nuncio Monseñor Sótero Sanz 100, Providencia, 7500011 Santiago, Chile
[14] Departamento de Astronomía, Universidad de Chile, Camino El Observatorio 1515, Las Condes, Santiago, Chile
[15] European Southern Observatory, Karl-Schwarzschild-Str. 2, D-85748 Garching b. München, Germany
[16] Departamento de Astrofísica y CC. de la Atmósfera, Facultad de CC. Físicas, UCM, Avda. Complutense s/n, E-28040 Madrid, Spain
[17] Department of Physics, Institute for Astronomy, ETH Zürich, CH-8093 Zürich, Switzerland
[18] Instituto de Astrofisíca, Facultad de Física, Pontificia Universidad Católica de Chile, Casilla 306, Santiago 22, Chile
[19] Australian Astronomical Observatory, P.O. Box 915, North Ryde, NSW 1670, Australia
[20] Department of Physics and Astronomy, Macquarie University, Sydney, NSW 2109, Australia
Received 2015 September 17; accepted 2016 February 8; published 2016 April 19

ABSTRACT

The "main sequence of galaxies"—defined in terms of the total star formation rate ψ versus the total stellar mass M_*—is a well-studied tight relation that has been observed at several wavelengths and at different redshifts. All earlier studies have derived this relation from integrated properties of galaxies. We recover the same relation from an analysis of spatially resolved properties, with integral field spectroscopic (IFS) observations of 306 galaxies from the CALIFA survey. We consider the SFR surface density in units of $\log(M_\odot\,\mathrm{yr}^{-1}\,\mathrm{Kpc}^{-2})$ and the stellar mass surface density in units of $\log(M_\odot\,\mathrm{Kpc}^{-2})$ in individual spaxels that probe spatial scales of 0.5–1.5 Kpc. This local relation exhibits a high degree of correlation with small scatter ($\sigma = 0.23$ dex), irrespective of the dominant ionization source of the host galaxy or its integrated stellar mass. We highlight (i) the integrated star formation main sequence formed by galaxies whose dominant ionization process is related to star formation, for which we find a slope of 0.81 ± 0.02; (ii) for the spatially resolved relation obtained with the spaxel analysis, we find a slope of 0.72 ± 0.04; and (iii) for the integrated main sequence, we also identified a sequence formed by galaxies that are dominated by an old stellar population, which we have called the retired galaxies sequence.

Key words: galaxies: evolution – galaxies: fundamental parameters – galaxies: star formation

1. INTRODUCTION

Thanks to the increasing number of statistical studies of both local and distant galaxies, it has been possible to reveal and confirm several correlations in extragalactic astronomy. One of these relations is the so-called star formation main sequence (SFMS) of actively star-forming galaxies, which relates the star formation rate (SFR, ψ) and the stellar mass (M_*).

The SFMS is an approximately linear correlation between $\log\psi$ and $\log M_*$ that has been observed in the local universe as well as at high redshifts. See, for example, Brinchmann et al. (2004), Salim et al. (2007), and Renzini & Peng (2015, hereafter RP15) for $z \sim 0$; Peng et al. (2010) for $z \lesssim 1$; and Daddi et al. (2007, hereafter D07) for $z > 1$. In particular, Speagle et al. (2014, hereafter S14) performed a compilation of SFMS relations reported in the literature and showed a summary of the evolutionary behavior of the SFMS with redshift (up to $z \sim 6$). Katsianis et al. (2015) performed a similar study of the evolution of this correlation for $z \sim 1$–4. The SFMS is also recovered in cosmological simulations (Davé et al. 2011; Torrey et al. 2014; Sparre et al. 2015, hereafter S15). In fact, this correlation has been proven to be tight, with a scatter of ∼0.2–0.35 dex in observations and in theoretical predictions (D07; S15; S14). The values of the slope and zero points for the SFMS may vary within a large range in the literature (see S14 for a compilation). It has been proposed that these variations may originate from the selection criteria used to select star-forming galaxies. RP15 has proposed a new objective definition for the SFMS for local galaxies, which favors values of 0.76 dex and -7.64 $\log(M_\odot\,\mathrm{yr}^{-1})$ for the slope and zero points, respectively.

Although the physical distinction between star-forming and passive galaxies is not straightforward (see, e.g., Casado et al. 2015), the SFMS correlation provides a convenient way to classify galaxies in terms of their SF properties. Generally, the star-forming galaxies lie on the main sequence, red elliptical galaxies tend to lie below the relation, while the starburst galaxies lie above the sequence (S15).

All previous SFMS studies have been done using integrated quantities for the galaxies. Due to observational restrictions, the derivation of quantities like SFR and M_* have been performed using, for example, single fiber spectroscopy affected by aperture losses that need to be corrected. Integral field spectroscopy (IFS) allows us to have spatial and spectroscopical information for extended objects, as it delivers individual spectra for each point of the observed target (restricted to the instrument spatial resolution), which makes IFS a suitable observational technique for studying spatially resolved physical quantities in galaxies. Studying the SFMS with IFS would allow us to obtain both integrated and local correlations. If the field of view covers the entire optical extension of the galaxy, these data are not affected by aperture loss.

IFS, when used to perform sky surveys, allows us to perform statistical studies of spatially resolved physical quantities of galaxies. The Calar Alto Legacy Integral Field Area survey (CALIFA; Sánchez et al. 2012) is an ongoing extragalactic optical IFS survey designed to observe around 600 galaxies, which makes it suitable for performing spatially resolved studies with statistical significance.

We present the results of studying the spatially resolved SFMS based on data from the CALIFA survey. Throughout this paper, we have adopted a Salpeter IMF and a cosmology defined by $H_0 = 71\,\mathrm{km\,s^{-1}\,Mpc^{-1}}$, $\Omega_\Lambda = 0.7$, and a flat universe.

2. DATA AND SAMPLE OF GALAXIES

We used the available sample observed by CALIFA until 2015 February, consisting of 535 galaxies that are representative of its mother sample (Walcher et al. 2014; mass and redshift ranges are $10^{9.7} < M_* < 10^{11.4} M_\odot$ and $0.005 < z < 0.03$, respectively), which includes galaxies of all morphological types, inclinations, and environments. Galaxies from CALIFA extended samples observed as ancillary programs, i.e., galaxies not contemplated in the original mother sample, were also included. For this reason, the M_* of some of the galaxies in our sample may be lower than the limits established on the mother sample. In order to avoid inclination effects, we clipped our sample to a low-inclination (i) galaxy subsample with $i < 60°$, for which 306 galaxies remained.

The observations were performed using the PMAS instrument (Roth et al. 2005) in the PPAK configuration (Kelz et al. 2006). The observing strategy guarantees a complete coverage of the spatial extension of the galaxies up to 2.5 effective radius, with an FWHM $\sim 2\farcs5$ (García-Benito et al. 2015), which corresponds to $\sim$1 kpc at the average redshift of the survey (for further information of the survey, sample, and observational strategy, see Sánchez et al. 2012)

We used data from the V500 setup that cover a wavelength range of 3745–7300 Å, with a nominal resolution of $\lambda/\Delta\lambda = 850$ at 4500 Å. The data cubes were provided by version 1.5 of the pipeline (García-Benito et al. 2015) and consist of a regular grid of 72 × 78 spectra, with a $1''$/spaxel size centered in the galaxies.

3. SFRs AND STELLAR MASS CALCULATION

The data cubes were analyzed using the Pipe3D pipeline (Sánchez et al. 2016), which is a tool that fits the continuum with stellar population models and measures the nebular emission lines. This pipeline is based on the Fit3D fitting tool (Sánchez et al. 2015). For this particular implementation, we adopted the GSD156 library of simple stellar population models (Cid Fernandes et al. 2013, hereafter CF13) that comprises 156 templates covering 39 stellar ages (from 1 Myr to 13 Gyr) and 4 metallicities ($Z/Z_\odot = 0.2$, 0.4, 1, and 1.5). These templates have been extensively used within the CALIFA collaboration (e.g., Pérez et al. 2013; González Delgado et al. 2014; CF13). Details of the fitting procedure, dust attenuation curve, and uncertainties of the process are given in Sánchez et al. (2015, 2016).

We applied a spatial binning to each data cube to reach a homogeneous S/N of 50 across the field of view. Then, the stellar population fitting was applied to the coadded spectra within each spatial bin. Finally, following the procedures described in CF13 and Sánchez et al. (2015), we derive the stellar population model for each spaxel by re-scaling the best-fitted model within each spatial bin to the continuum flux intensity in the corresponding spaxel. The stellar population model is then subtracted to create a gas-pure cube comprising only the ionized gas emission lines. Thus, it is assumed that the same M/L ratio and dust attenuation for those spaxels within the same spatial bin derive a spaxel-wise map of any stellar property, like the M_* surface density (Σ_*).

For the gas-pure cube, the strongest emission lines within the considered wavelength range, including Hα and Hβ, are fitted spaxel-by-spaxel to derive their corresponding flux intensity and equivalent width (EW) maps. The Hα flux is then corrected by the ionized gas dust attenuation, derived using the Balmer decrement assuming a canonical value of 2.86, adopting a Cardelli et al. (1989) extinction law and $R_v = 3.1$. The Hα luminosity distribution is derived by correcting for the cosmological distance, and by applying the Kennicutt (1998) conversion from Hα luminosity to SFR, we derive both the integrated SFRs and the spaxel-wise distribution of the SFR surface density (μSFR). The measured μSFR and Σ_* have not been corrected for galaxy inclination. However, since we have limited our sample to galaxies with $i < 60°$, the impact of inclination on the projected surface densities will be less than a factor of two.

4. RESULTS

The procedure described in Section 3 was applied to the 306 galaxies mentioned in Section 2 to construct the SFMS relation for the CALIFA sample.

4.1. Integrated SFMS Relation

Figure 1 shows the integrated M_* versus SFR relation that was constructed integrating the corresponding spatially resolved quantities of all the galaxies in the sample. Preliminary versions of this plot for smaller subsamples of the CALIFA data already have been presented in Sánchez et al. (2013) and Catalán-Torrecilla et al. (2015).

In Figure 1, we classify the dominant ionization source in the galaxies based on a combination of EW(Hα) classification, introduced by Cid Fernandes et al. (2011) and a classification using the Kewley demarcation limit (KL; Kewley et al. 2001) in the Baldwin–Phillips–Terlevich (BPT) diagram (Baldwin et al. 1981): (i) the green symbols account for galaxies for which the [O III]/Hβ and [N II]/Hα line ratios of their

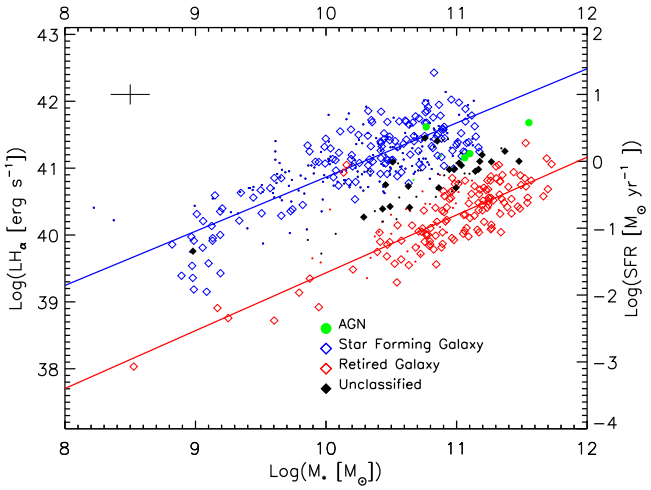

Figure 1. Integrated M_* vs. SFR relation for the CALIFA sample. Green symbols represent galaxies that lie above the Kewley limit (KL) and whose Hα equivalent widths (EWs) are >6 Å, i.e., are galaxies whose ionization emission is dominated by the AGN activity. Blue symbols represent galaxies below the KL and with EW(Hα) > 6 Å, and that have inclinations < 60°, i.e., that lie in the star formation main sequence (SFMS). Red symbols represent galaxies with EW(Hα) < 3 Å, i.e., that lie in a retired galaxies sequence (RGS). Finally, black symbols account for galaxies whose EW(Hα) lies between 3 and 6 Å, i.e., galaxies whose dominant ionization process is uncertain. Shaped symbols hold for galaxies in the low-inclination subsample that are the ones used for the rest of the analysis; however, for completeness, the points show the complementary high-inclination subsample. Blue and red lines are the linear fittings to the SFMS for low inclined galaxies and RGS, respectively (see Table 1 for details). SFRs shown in the plot only hold for the SF-dominated galaxies, for the rest these rates are only the result of the linear transformation of the Hα luminosities with the Kennicutt (1998) relation. For further details of the galaxy classifications, please refer to Section 4.1.

integrated ionized gas emission lines lie above the KL and whose EW(Hα) are >6 Å, meaning that the dominant ionization process in these galaxies comes from the nuclear activity. (ii) The blue symbols represent the galaxies that lie below the KL in the BPT diagram, and whose EW(Hα) are >6 Å, which means that the ionization processes in these galaxies are dominated by SF, as shown in Figure 3 of Sánchez et al. (2014). (iii) The red symbols account for galaxies whose EWs(Hα) are <3 Å regardless of their position in the BPT diagram, meaning that most of the dominant processes in the gas ionization probably come from an old stellar population (Cid Fernandes et al. 2011). (iv) Finally, black symbols represent galaxies whose EWs(Hα) are 3 Å < EW < 6 Å, which means that their main ionization processes remain uncertain. Shaped symbols account for the galaxies from the low i subsample, which are the ones used for the rest of the analysis. For completeness, points show the galaxies for the complementary high i subsample.

Although we have transformed the Hα luminosities to SFRs for all the galaxies adopting the Kennicutt (1998) relation, we should clarify that the interpretation of SFRs is only valid for galaxies (and regions) that are ionized by young stars (following our previous criteria). For the rest of the galaxies, the SFRs presented in the plot are indeed just a linear transformation of the Hα luminosity.

For the star-forming and retired galaxy sequences (blue and red, respectively), which from now on will be referred to as SFMS and retired galaxy sequence (RGS), we have fitted linear correlations between $\log(\psi)$ and $\log(M_*)$, whose characteristics are listed in Table 1, along with their dispersions. The slope and zero point for the SFMS are in good agreement with the values reported in the literature for local galaxies (RP15, S14 and references therein; for further details, see Section 5). For the black and green points, no further analysis was performed due to the uncertain main ionization process of the gas and due to its poor statistics, respectively.

The uncertainties of the derived quantities are dominated by the spectrophotometric accuracy of the CALIFA data, which is estimated to be ~6% (García-Benito et al. 2015), as well as the details of the procedure followed to derive the M_* and the SFRs. In the case of M_*, it has been determined that the uncertainties are well constrained within a typical error of ~0.15 dex (see, e.g., the discussion in Sánchez et al. 2013). The typical sizes of the uncertainties for our data are shown in Figure 1, which are consistent with what was previously found by Cid Fernandes et al. (2014) and Catalán-Torrecilla et al. (2015), and were taken into account when computing the linear fitting.

4.2. Spatially Resolved SFMS Relation

Next, we explore the spatially resolved SFMS for the CALIFA sample by plotting the SFR surface density versus the M_* surface density in Figure 2. The individual spaxels used in constructing the relation have spatial scales of 0.5–1.5 kpc that are larger than typical H II region sizes (hundreds of parsecs; González Delgado & Pérez 1997). It was derived using only the spaxels that fulfill the same criteria as the blue points in Figure 1, irrespective of the location of its host galaxy in that figure. Indeed, 11% of the included spaxels come from galaxies for which the global ionization is not dominated by SF (i.e., not blue in Figure 1).

A density plot of the local SFMS, based on 90,786 individual spectra, is shown in Figure 2. Colors account for the density of data points, and the yellow line represents a linear fitting to the correlation using only the 80% of the data, corresponding to the data contained inside the largest contour in the density plot that corresponds to the linear regime of the data. However, in Table 1, we present the results of the fitting using both 100% and 80% of the data. The fitting was performed using variable mass bins that individually contain 1% of the total amount of data and shows that the spatially resolved SFMS relation holds in general as a linear relation. Uncertainties in this plot are not shown, but were taken into account in the computation of the linear fitting and are reflected in the errors of the slope and zero point of the correlation.

The spatially resolved SFMS proves to be a tight correlation, as the standard deviation (σ) is quite small $\sigma = 0.23$ dex, comparable to the value obtained for the integrated relation, in this work and previous independent studies (see, for example, D07; S14; S15).

5. DISCUSSION

In Section 4.1, we explored the tight correlation between the SFR (inferred from Hα luminosity) and the total M_* for star-forming (SFMS) and retired (RGS) galaxies in logarithmic scales. In the case of the integrated SFMS the slope and zero point (see Table 1) are in good agreement with the previously reported values. Even if the range of variation of reported slopes and zero points in the literature may be as large as ~0.4–1 for the slope and ~−(4–10) for the zero points for local galaxies (S14), many recent works tend to constrain these

Table 1
Relevant Intrinsic Coefficients of the Integrated SFMS and RGS Relations and of the Spatially Resolved SFMS Relation, as Well as Those Derived by a Linear Regression Procedure to Each of Them

Coefficient	SFMS	RGS	Spatially Resolved SFMS 100% of the Data	Spatially Resolved SFMS 80% of the Data
Pearson Correlation Coeff. (ρ)	0.84	0.85	0.61	0.63
ρ99% Confidence Interval	(0.76, 0.89)	(0.77, 0.90)	(0.60, 0.61)	(0.62, 0.63)
Slope	0.81 ± 0.02	0.86 ± 0.02	0.68 ± 0.04	0.72 ± 0.04
Zero Point	-8.34 ± 0.19[a]	-10.32 ± 0.24[a]	-7.63 ± 0.34[b]	-7.95 ± 0.29[b]
Standard Deviation (σ)	0.20	0.22	0.23	0.16

Notes. The σ value is the deviation about the fitting.
[a] Units: [$\log(M_\odot\ \mathrm{yr}^{-1})$].
[b] Units: [$\log(M_\odot\ \mathrm{yr}^{-1}\ \mathrm{Kpc}^{-2})$].

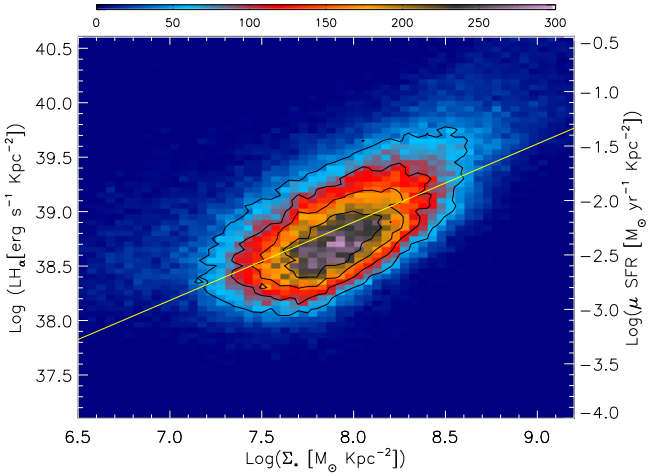

Figure 2. Spatially resolved SFMS relation for the CALIFA sample that holds for scales in the range of 0.5–1.5 kpc. Colors in the plot represent the amount of data points presented in this study. The outermost contour holds within itself 80% of the total data presented in the plot. Further contours hold 60%, 40%, and 20% of the total amount of data in the plot. Yellow line represents the linear fitting to the spatially resolved SFMS relation using the 80% of the data (see Table 1 for further details of the linear fitting).

values to smaller ranges, such as 0.71–0.77 and −(6.78–7.64) (Elbaz et al. 2007; Zahid et al. 2012; RP15). Even more, published dispersions of this relation (∼0.2–0.35 dex) are in good agreement with the dispersion found with our data (0.20 dex).

In Section 4.2, we presented the spatially resolved SFMS relation. The observed correlation holds on kiloparsec scales and is consistent with the slope of 0.66 ± 0.18 reported by Sánchez et al. (2013) for H II regions. Comparing the integrated and the spatially resolved relations, our results (summarized in Table 1) indicate that not only the slopes, but also the intrinsic scatter, are roughly of the same order in both relations.

We explored the local relation in different M_* bins, finding that it has no dependence on this parameter. We fitted linear correlations to each mass bin relation and used a 2D Kolmogorv–Smirnov test to verify that the spatially resolved SFMS present the same distribution irrespective of the mass of the host galaxy; however, we will explore this in more detail in further works. We also explored the possible effects in the local SFMS determination, relaxing our criteria to select the SF regions by allowing the regions laying below the KL and whose EWs(Hα) are <3 to be considered also as SF regions. From this test, we found that for both relations, using the 100% and 80% of the data, the slope varies just ∼0.04 dex, i.e., it has a little impact in our results.

From a physical point of view, we know that SF is a local process, and therefore it is not unreasonable that the scaling relations governing it are local as well. The fact that the SFMS relation remains as a tight linear correlation on kiloparsec scales suggests that the conversion of gas into stars is mainly driven by local rather than global processes.

A local SFMS could only be derived from the global one if the spatial distribution of both the μSFR and Σ_* followed similar patterns in all galaxies. Given the variations in the shape and normalization of these observed profiles (e.g., González Delgado et al. 2015; R. M. González Delgado et al. 2016, in preparation), it seems rather fine-tuned that a mechanism acting on the scale of the whole galaxy affects both surface densities exactly in the way required to yield a universal relation on resolved scales without a local process being involved.

To recover the global relation from the local one, we just need to integrate the resolved quantities across the whole area of the galaxy. In terms of the stellar mass surface density Σ_h at the half-light radius R_h, the total stellar mass should roughly scale as $M_* \propto \Sigma_h R_h^2$. If the star formation surface density fulfills $\mu_{\mathrm{SFR}} \propto \Sigma_*^{\gamma}$ at every point (i.e., a local SFMS with logarithmic slope γ), one obtains the integrated relation $\psi \propto \Sigma_h^{\gamma} R_h^2 = \Sigma_h^{\gamma-1} M_*$. Since $\Sigma_h \propto M_*^{\beta}$ with $\beta \sim 0.5$ (e.g., Kauffmann et al. 2003; González Delgado et al. 2015), the logarithmic slope of the integrated SFMS would be

$$\alpha = 1 + (\gamma - 1)\beta \sim 1 - 0.3 \times 0.5 = 0.85 \qquad (1)$$

if it was a consequence of the local relation. If Equation (1) holds, $\alpha - \gamma = (1 - \beta)(1 - \gamma) > 0$ implies that the integrated SFMS should be slightly steeper than the local relation, in rough agreement with the results reported in Table 1.

It must be noted, though, that this prediction is only valid if $M_* \propto \Sigma_h R_h^2$, which is merely a first-order approximation. Moreover, the measured value of the logarithmic slope α is rather sensitive to the sample selection criteria (inclination, EW threshold, etc.), and we have to keep in mind that the galaxies used in the integrated relation, even if they were selected for being dominated by the SF activity, may contain local zones that are not star forming.

6. CONCLUSIONS

We report the spatially resolved SFMS relation using IFS data from the CALIFA survey that holds for kiloparsec scales. Our sample consists of galaxies of mixed morphological types and masses that extend to three orders of magnitude. M_*

have been derived from stellar population fits to optical spectra, and SFRs have been inferred from the extinction-corrected intensity of the Hα emission line.

For an integrated SFR versus M_* plot, we identified two main sequences, one accounts for the RGS and the other for the SFMS itself; for this last one, we report a slope of 0.81 ± 0.02 and a dispersion of 0.20 dex. For the star-forming areas in each galaxy, irrespectively of their integrated properties, we find a correlation between the μSFR and the Σ_* that is as tight as the integrated one, and that seems to be the fundamental relation from which the global one is derived. For the local SFMS, we found a slope of 0.72 ± 0.04 and a dispersion of 0.23 dex.

In future articles, we will explore the possible dependence of this relation on other properties of the galaxies, like morphology, color, environment, etc., as well as the derivation of the spatially resolved RGS

We acknowledge the referee, E. Pérez, and R. Cid Fernandes for their comments. Financial support: M.C.D. and S.F.S.: DGAPA-UNAM funding; CONACyT-180125 and PAPIIT IA-100815 projects. Z.S.: EU Marie Curie Career Integration Grant "SteMaGE" PCIG12-GA-2012-326466. Y.A.: RyC-2011-09461 and AYA2013-47742-C4-3-P projects from the Spanish MINECO and the SELGIFS programme, funded by the EU (FP7-PEOPLE-2013-IRSES-612701). C.J.W.: Marie Curie Career Integration Grant 303912. R.M.G.D.: AyA2014-57490-P and J.A. P12-FQM2828 grants. J.F.B.: AYA2013-48226-C3-1-P from the Spanish MINECO grant. L.G.: Millennium Science Initiative through grant IC120009, and by CONICYT through FONDECYT grant 3140566.

REFERENCES

Baldwin, J. A., Phillips, M. M., & Terlevich, R. 1981, PASP, 93, 5
Brinchmann, J., Charlot, S., White, et al. 2004, MNRAS, 351, 1151
Cardelli, J. A., Clayton, G. C., & Mathis, J. S. 1989, ApJ, 345, 245
Casado, J., Ascasibar, Y., Gavilán, M., et al. 2015, MNRAS, 451, 888
Catalán-Torrecilla, C., Gil de Paz, A., Castillo-Morales, A., et al. 2015, A&A, 584, A87
Cid Fernandes, R., González Delgado, R. M., García Benito, R., et al. 2014, A&A, 561, A130
Cid Fernandes, R., Pérez, E., García Benito, R., et al. 2013, A&A, 557, A86
Cid Fernandes, R., Stasińska, G., Mateus, A., & Vale Asari, N. 2011, MNRAS, 413, 1687
Daddi, E., Dickinson, M., Morrison, G., et al. 2007, ApJ, 670, 156
Davé, R., Oppenheimer, B. D., & Finlator, K. 2011, MNRAS, 415, 11
Elbaz, D., Daddi, E., Le Borgne, D., et al. 2007, A&A, 468, 33
García-Benito, R., Zibetti, S., Sánchez, S. F., et al. 2015, A&A, 576, A135
González Delgado, R. M., & Pérez, E. 1997, ApJS, 108, 199
González Delgado, R. M., Cid Fernandes, R., García Benito, R., et al. 2014, ApJL, 791, L16
González Delgado, R. M., García-Benito, R., Pérez, E., et al. 2015, A&A, 581, A103
Katsianis, A., Tescari, E., & Wyithe, J. S. B. 2015, arXiv:1508.01615
Kauffmann, G., Heckman, T. M., White, S. D. M., et al. 2003, MNRAS, 341, 54
Kelz, A., Verheijen, M. A. W., Roth, M. M., et al. 2006, PASP, 118, 129
Kennicutt, R. C., Jr. 1998, ARA&A, 36, 189
Kewley, L. J., Dopita, M. A., Sutherland, R. S., et al. 2001, ApJ, 556, 121
Peng, Y.-j., Lilly, S. J., Kovač, K., et al. 2010, ApJ, 721, 193
Pérez, E., Cid Fernandes, R., González Delgado, R. M., et al. 2013, ApJL, 764, L1
Renzini, A., & Peng, Y.-J. 2015, ApJL, 801, L29
Roth, M. M., Kelz, A., Fechner, T., et al. 2005, PASP, 117, 620
Salim, S., Rich, R. M., Charlot, S., et al. 2007, ApJS, 173, 267
Sánchez, S. F., Kennicutt, R. C., Gil de Paz, A., et al. 2012, A&A, 538, AA8
Sánchez, S. F., Pérez, E., Sánchez-Blázquez, P., et al. 2015, RMxAA, in press (arXiv:1509.08552)
Sánchez, S. F., Pérez, E., Sánchez-Blázquez, P., et al. 2016, RMxAA, in press (arXiv:1602.01830)
Sánchez, S. F., Rosales-Ortega, F. F., Jungwiert, B., et al. 2013, A&A, 554, A58
Sánchez, S. F., Rosales-Ortega, F. F., Iglesias-Páramo, J., et al. 2014, A&A, 563, A49
Sparre, M., Hayward, C. C., Springel, V., et al. 2015, MNRAS, 447, 3548
Speagle, J. S., Steinhardt, C. L., Capak, P. L., & Silverman, J. D. 2014, ApJS, 214, 15
Torrey, P., Vogelsberger, M., Genel, S., et al. 2014, MNRAS, 438, 1985
Walcher, C. J., Wisotzki, L., Bekeraité, S., et al. 2014, A&A, 537, A1
Zahid, H. J., Dima, G. I., Kewley, L. J., et al. 2012, ApJ, 757, 54